Ion temperature gradient instability at sub-Larmor radius scales with non-zero ballooning angle

P. Migliano[1], Y. Camenen[2], F.J. Casson[3], W.A. Hornsby[1], A.G. Peeters[1]
[1] *University of Bayreuth, Physics department, Universitätsstrasse 30 Bayreuth, Germany*
[2] *Aix-Marseille Université, CNRS, PIIM UMR 7345, 13397 Marseille, France and*
[3] *Max Planck Institut fuer Plasmaphysik, EURATOM association, Boltzmannstrasse 2, 85748 Garching, Germany*

Linear gyro-kinetic stability calculations predict unstable toroidal Ion Temperature Gradient modes with normalised poloidal wave vectors well above one ($k_\theta \rho_i > 1$) for standard tokamak parameters with adiabatic electron response. These modes have a maximum amplitude at a poloidal angle θ that is shifted away from the low field side ($\theta \neq 0$). The physical mechanism is clarified through the use of a fluid model. It is shown that the shift of the mode away from the low field side reduces the effective drift frequency which allows for the instability to develop. Numerical tests using the gyro-kinetic model confirm this physical mechanism. Furthermore it is shown that modes localized away from the low field side can be important also for $k_\theta \rho_i < 1$ close to the threshold of the ITG. In fact, modes with maximum amplitude at $\theta \neq 0$ can exist for normalised temperature gradient lengths below the threshold of the ITG obtained for the case with the maximum at $\theta = 0$.

PACS numbers: 52.25.Fi, 52.25.Xz, 52.30.Gz, 52.35.Qz, 52.55.Fa

I. INTRODUCTION

The growth rate of the ion temperature gradient mode (ITG) as a function of the normalised poloidal wave vector $k_\theta \rho_i$, has been reported many times in the literature, see for instance [1], as a bell shaped curve with a single maximum. Here, k_θ is the poloidal component of the wave vector and $\rho_i = m_i v_{thi}/ZeB = \sqrt{2 m_i T_i}/ZeB$ is the ion Larmor radius, with m_i the ion mass, v_{thi} the ion thermal velocity, Z the charge number, e the elementary charge, B the magnetic field strength, and T_i the ion temperature.

In this paper we report on collisionless Ion Temperature Gradient (ITG) instabilities with $k_\theta \rho_i > 1$ and adiabatic electrons. It will be shown that these instabilities can exist for relevant Tokamak parameters. The physical mechanism of these instabilities will be shown to be related to the reduction of the effective drift frequency through the shift of the mode away from the low field side position. This mechanism is different from those previously reported [2–6] with $k_\theta \rho_i > 1$, which are unstable only in a slab or for weak toroidicity.

This paper is structured as follows: Section II introduces the high k_θ ITG through numerical simulation based on the gyro-kinetic model, Section III discusses the physics of the instability through the use of a simple fluid model. Section IV discusses the relation with previously published work, and finally Section V gives the conclusions.

II. HIGH k_θ ITG

In this paper all simulations are performed using the local limit or flux tube approximation [7]. *This limit considers a radial domain around a local flux surface that is sufficiently small such that all plasma as well as all geometry parameters can be taken to be uniform in the radial direction. The local limit allows for a spectral approach in the radial direction, and is equivalent to the ballooning transform [8] (the use of ballooning transform below is referred as the "spectral case") when only terms of lowest significant order in the normalized Larmor radius are considered. The ballooning transform, however, is often utilised in a restrictive manner, by choosing the radial wave vector zero at the low field side. A choice motivated by the observation that this usually yields the most unstable mode.* An example of a calculation using this restrictive form of ballooning transform, obtained with the gyrokinetic code GKW [9, 10], is given in Fig. 1 by the dash-dotted (blue 'x') curve that has a single maximum. The parameters of this, and all other simulations in this paper, are those of the Waltz standard case [11]: ion temperature gradient length $R/L_{Ti} = 9.0$ density gradient length $R/L_{ni} = 3.0$, electron and ion temperature $T_e = T_i$, safety factor $q = 2$, magnetic shear $\hat{s} = 1$, and inverse aspect ratio $\epsilon = 0.166$. The simulations use circular geometry [12] retaining finite ϵ effects, and the flux tube approximation is always applied.

However, GKW simulations with the radial direction described using finite differences (simulations that use finite difference in the radial direction below are referred to as the "non-spectral case") show a surprisingly different behaviour for $k_\theta \rho_i > 0.6$, displaying a spectrum with two maxima and having unstable modes with $k_\theta \rho_i$ well above one, as is shown by the full (black) line of Fig. 1. The dashed line (red circles) in this figure is obtained *by choosing in the spectral runs the radial wave vector at the low field side that maximises the growth rate. This radial wave vector happens not always to be zero as will be explained in the follwing.*

The essential difference between these two simulations

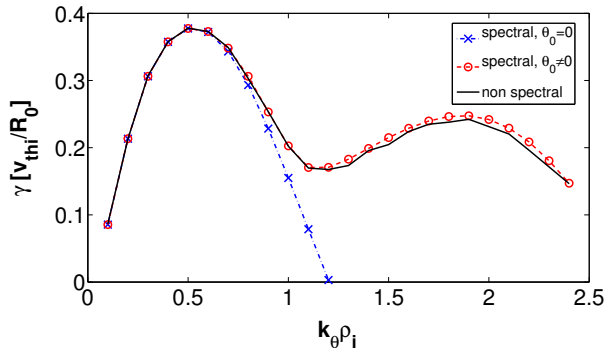

FIG. 1: (Colour on-line) Growth rate (γ in units v_{thi}/R_0 where R_0 is the major radius of the magnetic axis) as a function of $k_\theta\rho_i$. The dash-dotted (blue 'x') line is the spectral case with $\theta_0 = 0$, the solid (black) line is the non-spectral case, and the dashed (red circles) line is the maximum growth rated obtained when varying θ_0 in the spectral case.

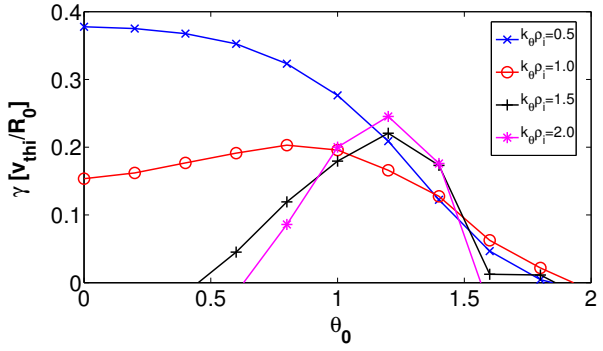

FIG. 2: (Colour on-line) Growth rates of the spectral case (γ in units v_{thi}/R_0) as a function of θ_0 for four representative values of $k_\theta\rho_i$. The curves are denoted as follows: $k_\theta\rho_i = 0.5$ (blue 'x') crosses, $k_\theta\rho_i = 1.0$ (red circles) circles, $k_\theta\rho_i = 1.5$ (black '+') pluses, $k_\theta\rho_i = 2.0$ (magenta stars)

is the number of radial modes that are kept. There are many more radial modes in the non-spectral case compared to the spectral one, in which the radial wave vector (k_r) is set by the condition of the field alignment of the mode [8]

$$k_r = \hat{s}\theta k_\theta \ , \tag{1}$$

which is zero at the low field side position (poloidal angle $\theta = 0$). This suggests that the unstable modes for $k_\theta\rho_i > 1$ have a finite radial wave vector at the low field side position. It is well known that a finite radial wave vector can be introduced in the ballooning transform through the introduction of the angle, θ_0, such that

$$k_r = \hat{s}(\theta - \theta_0)k_\theta \ . \tag{2}$$

The growth rate as a function of θ_0 for various values of $k_\theta\rho_i$ is shown in Fig. 2. For $k_\theta\rho_i > 0.6$ the most unstable mode has a finite θ_0 and the mode is shifted away from the low field side, as shown in Fig. 3, which displays the eigen function along the magnetic field for $k_\theta\rho_i = 1.5$ and $\theta_0 = 1.2$. There is no preferred sign for θ_0 and the mode with $\theta_0 = -1.2$ is equally unstable but shifted in the negative θ direction. Taking the maximum growth rate (by varying θ_0) for each $k_\theta\rho_i$ from the spectral simulations yields the dashed (red circles) curve in Fig. 1. There is the expected agreement between the spectral and the non-spectral cases.

In order to get further insight into the high k_θ ITGs several parameter scans have been performed. These are done by varying one parameter while keeping all the other parameters fixed to the standard case. The results of the R/L_T, q and $\hat{s}$ scans are shown in Figs. 4 and 5. All calculations are performed using the non-spectral setup with $k_\theta\rho_i = 1.9$. For comparison, the results for $k_\theta\rho_i = 0.5$ are also shown. Fig. 4 shows that the growth rate of

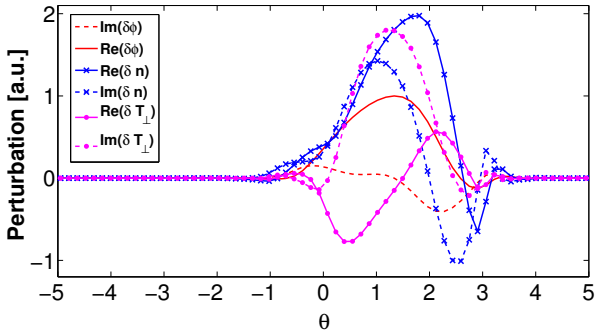

FIG. 3: (Colour on-line) Eigenfunction in arbitrary units as a function of the poloidal angle θ. *The figure is obtained from a spectral run with* $k_\theta\rho_i = 1.5$ *and* $\theta_0 = 1.2$. Solid lines give the real, whereas dashed lines give the imaginary part. The (red) lines without symbols is the potential perturbation ($\delta\phi$), the (blue) lines with the symbol 'x' the density perturbation (δn), and the (magenta) lines with the closed circles is the perpendicular temperature perturbation ($\delta T_\perp$).

the high k_θ ITG increases with R/L_T very similar to the $k_\theta\rho_i = 0.5$ mode. The mode has a higher threshold in R/L_T though it is more stable over the entire scan. In the same figure the dependence on the safety factor is also shown. A larger safety factor increases the connection length between the low and high field side increasing the time in which a perturbation propagates along the magnetic field line from the unfavourable curvature to the favourable curvature region. Therefore, increasing the safety factor has a destabilizing effect. This is the case for $k_\theta\rho_i = 0.5$, but to a much larger extent for the high k_θ ITG. The localisation of the mode at $\theta_0 \neq 0$ makes the requirement of a sufficient long field line length harder to satisfy.

Fig. 5 gives the value of the growth rate as a function

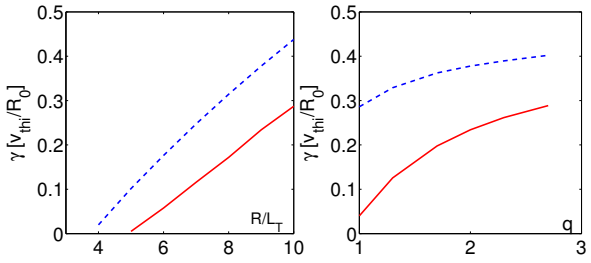

FIG. 4: (Colour on-line) The growth rate as a function of R/L_T (left) and the safety factor q (right) *for the non-spectral case*. The (red) full line gives the result for $k_\theta \rho_i = 1.9$, while the (blue) dashed line gives the result for $k_\theta \rho_i = 0.5$.

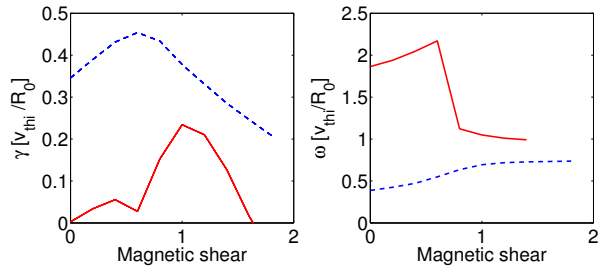

FIG. 5: (Colour on-line) The growth rate (left) and frequency (right) as a function of the magnetic shear *for the non-spectral case*. The (red) full line gives the result for $k_\theta \rho_i = 1.9$, while the (blue) dashed line gives the result for $k_\theta \rho_i = 0.5$.

of the magnetic shear. The growth rate curve has two maxima for $k_\theta \rho_i = 1.9$, and it can be verified from the figure of the frequency (right panel in Fig. 5) that these maxima belong to two different modes. *For low magnetic shear the mode is found to reach its maximum amplitude at the low field side (standard ITG with $\theta_0 = 0$). Indeed the frequency of this mode is high, and its growth rate is rather small. For high magnetic shear the mode is shifted away from the low field side (maximum amplitude at $\theta_0 = 1.2$).* A high growth rate is obtained only at sufficiently large shear. A high shear reduces the width in θ of the eigenmode and is therefore beneficial for the $\theta_0 \neq 0$ modes. As already pointed out, a large width in θ would mean that the mode has a significant amplitude in the favourable curvature region, which is stabilizing. At constant R (drifts roughly constant), the dependence of the growth rate on the inverse aspect ratio ϵ (not shown) is found to be relatively weak.

III. PHYSICAL MECHANISM

An understanding of the physics of the high k_θ ITGs can be obtained by considering a simple fluid model. Here, the equations and normalisation given in [13] are used, and the reader is referred to this paper for details on the derivation. The gyro-kinetic equation, neglecting the parallel derivatives can be written in the form (see Eq. (69) of Ref. [13]):

$$\frac{\partial f}{\partial t} + \mathbf{v}_D \cdot \nabla f = -\mathbf{v}_E \cdot \nabla_p F_M - \mathbf{v}_D \cdot \frac{Ze\nabla\langle\phi\rangle}{T} F_M \quad (3)$$

where $\mathbf{v}_D$ is the drift due to the magnetic field inhomogeneity, $\mathbf{v}_E$ is the perturbed ExB velocity, f the perturbed distribution function, ϕ the perturbed electrostatic potential, and ∇_p is defined through Eq. (70) of Ref. [13]. In comparison to Ref. [13] the plasma rotation will be neglected, but it will not be assumed that the mode is localised on the low field side. Assuming a concentric circular magnetic equilibrium and small inverse aspect ratio we have

$$\mathbf{v}_D \cdot \nabla = \mathrm{i} v_D k_\theta \cos\theta + \mathrm{i} v_D k_r \sin\theta = \mathrm{i} k_\theta v_D K \quad (4)$$

where θ is the poloidal angle, and k_θ (k_r) is the poloidal (radial) wave vector. In the equation above K is introduced to shorten the mathematics. Using Eq. (2) one obtains

$$K = \cos\theta + \hat{s}(\theta - \theta_0)\sin\theta \ . \quad (5)$$

K measures the dependence of the convective derivative $(\mathbf{v}_D \cdot \nabla)$ on the poloidal angle.

Starting from Eq. (3) one can follow the same procedure as outlined in Ref. [13] to obtain the equations for the perturbed density ($\tilde{n}$) normalised to the background density, and perturbed temperature ($\tilde{T}$) normalised to the background temperature. For singly charged ions, neglecting the plasma rotation the expressions are

$$\omega\tilde{n} + 2K\tilde{n} + 2K\tilde{T} = \langle\tilde{\phi}\rangle\left(\frac{R}{L_n} - 2K\right) \quad (6)$$

$$\omega\tilde{T} + \frac{4}{3}K\tilde{n} + \frac{14}{3}K\tilde{T} = \langle\tilde{\phi}\rangle\left(\frac{R}{L_T} - \frac{4}{3}K\right) \quad (7)$$

where ω is the frequency normalised to the drift frequency $\omega_D = -k_\theta T/eBR$, and $\tilde{\phi}$ here is the perturbed electrostatic potential normalised with e/T. Note that all terms that are due to the drift are proportional to K. We will therefore refer to $\omega_D^* = \omega_D K$ as the effective drift frequency.

The angle brackets in the equation above denote the gyro-average, or FLR effects, which will be modelled using the approximation

$$\langle\tilde{\phi}\rangle = \frac{\tilde{\phi}}{1 + (k_\perp\rho_i)^2/2} = F\tilde{\phi} \quad (8)$$

where F has been introduced to shorten the notation. Finally, the gyro-kinetic Poisson equation is solved assuming adiabatic electrons

$$\tilde{n} = \left(1 + \frac{1}{2}k_\perp^2\rho_i^2\right)\tilde{\phi} = G\tilde{\phi} \quad (9)$$

where the term proportional to $k_\perp^2$ is due to the polarization.

From the equations above, a dispersion relation can be derived of the form:

$$A\left(\frac{\omega}{K}\right)^2 + B\frac{\omega}{K} + C = 0 \tag{10}$$

where

$$A = G \tag{11}$$

$$B = \frac{20}{3}G + 2F - \frac{F}{K}\frac{R}{L_N} \tag{12}$$

$$C = \frac{20}{3}(F+G) + 2\frac{F}{K}\frac{R}{L_T} - \frac{14}{3}\frac{F}{K}\frac{R}{L_N} \tag{13}$$

The growth rate (γ) normalised to $|\omega_D|$ can be readily calculated

$$\gamma = \frac{\sqrt{2K}}{G}\sqrt{\frac{R}{L_T} - K\frac{R}{L_{Tcrit}}} \tag{14}$$

where the critical gradient is given by

$$\frac{R}{L_{Tcrit}} = \frac{1}{8}B^2 - \frac{10}{3}(1+G^2) + \frac{7}{3}\frac{1}{K}\frac{R}{L_N} \tag{15}$$

and we have used $FG = 1$.

Fig. 6 shows the results of the growth rate, normalised to $|\omega_D|$, of the fluid model as a function of θ for three values of $\theta_0 = 0, 0.5, 1.0$. The left panel shows the results for $k_\theta\rho_i = 0.5$, whereas the right panel shows the results for $k_\theta\rho_i = 1.3$. It can be seen that for $k_\theta\rho_i = 0.5$ the mode has a maximum growth rate for $\theta = 0$, whereas for $k_\theta\rho_i = 1.3$ the mode with $\theta_0 = 0$ is stable and the most unstable mode occurs in the case $\theta_0 = 1.0$ with maximum at $\theta \approx \theta_0$.

The figure of the growth rate shows that the largest growth rate at high $k_\theta\rho_i$ is obtained for $\theta \approx \theta_0$, i.e. for $k_r \approx 0$. Therefore, from now on the local growth rate of the fluid model at the location $\theta = \theta_0$ (at this location $k_r = 0$) is considered. The value of k_r does not increase the FLR and polarization stabilisation of the mode. Next, we clarify why the mode is strongly stabilised for $\theta_0 = 0$ and has its maximum growth rate for $\theta_0 \neq 0$. For $\theta \approx \theta_0$, $k_r = 0$ and $K = \cos\theta_0$. Therefore $K = 1$ at the low field side position ($\theta_0 = 0$) and decreases for $\theta_0 \neq 0$. Eq. (14) gives the dependence of the growth rate on K. If K, rather than θ_0, is treated as a free parameter, and the density gradient is chosen to be zero for simplicity $R/L_N = 0$, then a maximum in the growth rate is obtained for

$$K_M = \frac{1}{2}\frac{R/L_T}{R/L_{Tcrit}} \ . \tag{16}$$

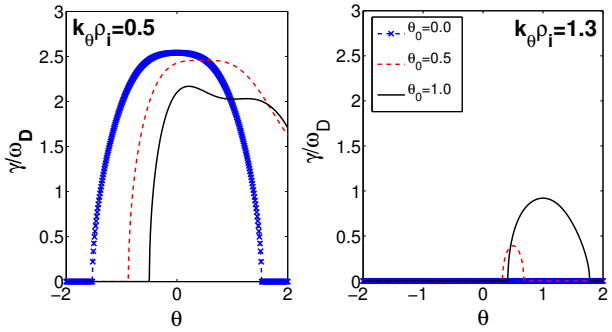

FIG. 6: (Colour on-line) Growth rates of the fluid model as a function of θ for $\theta_0 = 0$ (blue dashed 'x'), $\theta_0 = 0.5$ (red dashed) and $\theta_0 = 1.0$ (black solid). The left panel gives the growth rates for $k_\theta\rho_i = 0.5$, whereas the right panel gives the results for $k_\theta\rho_i = 1.3$. The values of θ_0 as well as the curve labels are the same for both panels.

i.e. when $R/L_T > 2R/L_{Tcrit}$ a maximum growth rate is obtained for the low field side position whereas for $R/L_T < 2R/L_{Tcrit}$ the maximum growth rate will be obtained for $\theta_0 \neq 0$. As $k_\theta\rho_i$ is increased for fixed R/L_T, R/L_{Tcrit} increases, K_M decreases, and the mode shifts away from the low field side. The dependence of γ on K is shown in Fig. 7 for various values of $k_\theta\rho_i$. It can be seen that for $k_\theta\rho_i = 0.5$ the low field side position is the position for which the maximum is reached, while it is shifted away from the low field side for $k_\theta\rho_i > 1$.

The physical reason for a maximum in K can be understood as follows. The ITG generates ion temperature perturbations due to the perturbed ExB velocity in the background gradients (the term proportional to R/L_T on the right hand side of Eq. (7)). Since the drift ($\mathbf{v}_D$) is a function of the particle energy, the temperature perturbations generate density perturbations through the convection (the term $2KT$ on the left hand side of Eq. (6)). These ion density perturbations then lead to the generation of the electric field (Eq. (9)) which is responsible for the perturbed ExB velocity. For $K = 0$, the convection due to the drift is zero and the mode is stable. One might therefore expect that a higher K leads to a more unstable mode, and to some extent this is indeed the case, as it is clear from the $\sqrt{2K}$ in the expression for γ in Eq. (14). However, the Eqs. (6,7) also contain terms that have a stabilising effect: the change in kinetic energy of the ions due to the drift motion in the perturbed potential (the term $-4K/3\langle\phi\rangle$ on the right hand side of Eq. (7)), the temperature perturbations that are generated by the perturbed density perturbations (the term $4Kn/3$ on the left hand side of Eq. (7)), and the fact that density and temperature perturbations have a tendency to propagate with different phase velocities (more physics explanations using diagrams can be found in [10]). These stabilising terms are responsible for the threshold of the

mode, and are all proportional to K. When the threshold is increased by FLR and polarization effects, and is close to R/L_T, the largest growth rate is obtained for $K < 1$, i.e. a mode shifted away from the low field side.

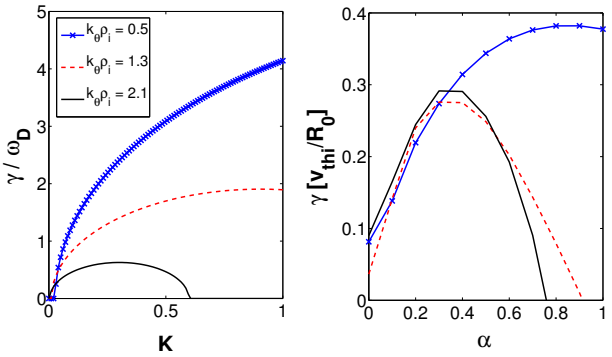

FIG. 7: (Colour on-line) Left panel: Growth rates (normalised to $|\omega_D|$) of the fluid model as a function of K for $k_\theta\rho_i = 0.5$ (blue solid 'x'), $k_\theta\rho_i = 1.3$ (red dashed), and $k_\theta\rho_i = 2.1$ (black solid). Right panel: Growth rates (normalised to v_{thi}/R_0) of spectral gyro-kinetic simulations with $\theta_0 = 0$, with the drift multiplied with a constant α. The values of $k_\theta\rho_i$ as well as the curve labels are the same as that of the fluid model in the left panel.

The fluid model is, of course, a strong simplification compared with the full gyro-kinetic model. The fluid model not only suggests that all instabilities close to the threshold would have their maximum growth rate away from the low field side, it also finds no threshold for the ITG, since for any finite R/L_T, K can be chosen small enough that an instability arises. In particular the parallel dynamics (Landau damping) contained in the gyro-kinetic model must be considered. This stabilising mechanism is independent of K and can be expected to stabilise any instability for which K is too small. Nevertheless, if the explanation based on the fluid model is correct, its predictions should be qualitatively reproducible by the gyro-kinetic simulations. We discuss two tests below.

First, we calculate the growth rate from the fluid model for different values of $k_\theta\rho_i$, treating K as a free parameter rather than θ_0 (as we did in the derivation of Eq. (16)). The outcome for the Waltz standard case parameters is shown in the left panel of Fig. 7. Indeed the fluid model reproduces qualitatively the same result given by the gyro-kinetic simulations, as can be seen comparing Figs. 7 and 2. *The fluid model suggests that the effect that leads to an increase in the growth rate is the reduction of the effective drift frequency.* To verify if the same physics mechanism is present also in the gyro-kinetic simulations, we can artificially multiply the drift velocity with a factor α ($0 \le \alpha \le 1$), in spectral simulations with $\theta_0 = 0$. This reduces the drift frequency and is as if we introduce the factor K of the fluid model into the gyro-kinetic simulations (with $\alpha = K$). The right panel of Fig. 7 shows the growth rates of the gyro-kinetic simulations as a function of α for the same values of $k_\theta\rho_i$ as the fluid model (shown in the left panel). *The scan in α is performed in the spectral case with $\theta_0 = 0$. In this case there is no shift of the mode away from the low field side.* For those modes that have a maximum growth rate when the mode is shifted away from the low field side, one expects the maximum growth rate for $\theta_0 = 0$ to be obtained for $\alpha < 1$, if the physics mechanism discussed above is correct. Indeed, the gyro-kinetic simulations at high $k_\theta\rho_i$ are stable for $\alpha = 1$ and have a maximum in the growth rate for $\alpha < 1$, qualitatively reproducing the fluid model.

Second, as discussed above, the mechanism is not limited to $k_\theta\rho_i > 1$. Close to the threshold, the most unstable mode can be expected to be shifted away from the low field side (provided the Landau damping is small enough). Fig. 8 shows the growth rate as a function of θ_0 of the Waltz standard case with $k_\theta\rho_i = 0.5$ for several values of R/L_T close to the threshold of the mode. Although the effect is small, the largest growth rate is obtained for $\theta_0 \neq 0$. In fact, for $R/L_T = 3.7$, an unstable mode exists for $\theta_0 \neq 0$ whereas the mode at $\theta_0 = 0$ is stable, i.e. a mode shifted away from the low field side exists for a temperature gradient length below the threshold of the ITG obtained for $\theta_0 = 0$. Both tests give confidence that the physical mechanism found through the analytic fluid model is indeed the reason for the observed behaviour of the gyro-kinetic simulations.

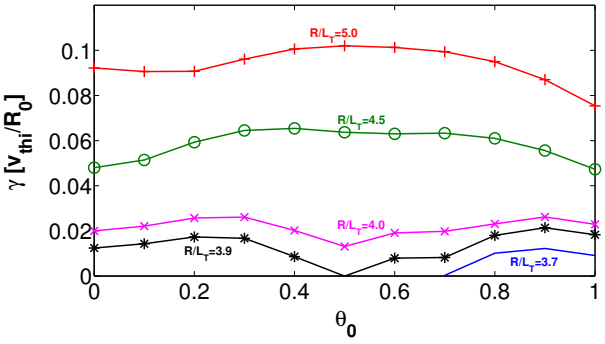

FIG. 8: (Colour on-line) Growth rates as a function of θ_0 *(spectral case)* for the Waltz standard case with $k_\theta\rho_i = 0.5$, and $R/L_T = 3.7$ (blue no symbols), $R/L_T = 3.9$ (black stars), $R/L_T = 4.0$ (magenta 'x'), $R/L_T = 4.5$ (green open circles), and $R/L_T = 5.0$ (red '+').

IV. COMPARISON WITH PREVIOUS WORK

Ion temperature gradient instability at sub-Larmor radius scales have previously been reported in the literature [2–6]. These modes have been found in slab geometry, as well as in the case of weak toroidicity. The latter condition translates to a density gradient $R/L_N > 6$ for the

instability to occur [3, 6]. Such a high gradient is not usually obtained in Tokamak plasmas under normal operation. In contrast, the high $k_\theta \rho_i$ ITG described in this paper occurs for a wide range of R/L_n as shown in Fig. 9, and is unstable for $R/L_n = 0$.

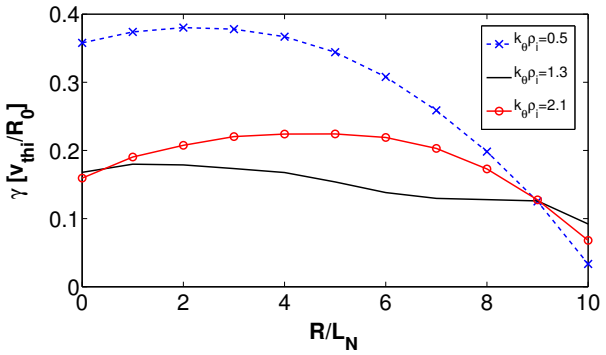

FIG. 9: (Colour on-line) Growth rates as a function of R/L_N *(non-spectral case)* for $k_\theta \rho_i = 0.5$ (blue dashed 'x'), $k_\theta \rho_i = 1.3$ (black solid), and $k_\theta \rho_i = 2.1$ (red open circles).

There are similarities between previous work and ours. In Refs. [2, 3] it is stressed that the non adiabatic response of the ions at $k_\theta \rho_i > 1$ is essential for the instability to occur. A similar statement can be made for the modes discussed in this paper. However, the essential ingredient discussed in this paper, the shift of the mode away from the low field side, reducing the effective drift frequency, is a distinct mechanism from that of the works published to date. In particular, an inspection of the equations in Refs. [2, 3, 5] shows that all these references assume $\theta_0 = 0$. We would like to point out that there are many numerical models [2, 3, 5, 6, 11, 14–16] that include the necessary physics to generate these shifted modes, and double humped structures have been observed on several occasions, even though the physics mechanism was not completely clarified.

V. CONCLUSION

In this paper we have shown that:

- The ITG with adiabatic electrons for standard tokamak parameters can be unstable for $k_\theta \rho_i$ substantially larger than one.
- Essential for this instability is a reduction of the effective drift frequency through the shift of the mode away from the low field side.
- An enhancement of the growth rate through the reduction of the effective drift frequency can be important for $k_\theta \rho_i < 1$, in particular close to the mode threshold.
- Unstable modes with $\theta_0 \neq 0$ can exist for ion temperature gradient lengths below the threshold of the mode obtained with $\theta_0 = 0$.

The existence of these modes might set additional requirements on resolution in nonlinear runs, and might play a role in small scale zonal flow generation.

Acknowledgement

Discussions with R. Singh and S. Brunner are gratefully acknowledged.

[1] A.M. Dimits, G. Bateman, M.A. Beer, B.I. Cohen, W. Dorland, G.W. Hammett, C. Kim, J.E. Kinsey, M. Kotschenreuther, A.H. Kritz, L.L. Lao, J. Mandrekas, W.M. Nevins, S.E. Parker, A.J. Redd, D.E. Shumaker, R. Sydora, J. Weiland, Physics of Plasmas **7** 969 (2000)
[2] A.I. Smolyakov, M. Yagi, and Y. Kishimoto, Phys. Rev. Lett. **89**, 125005 (2002)
[3] A. Hirose, M. Elia, A.I. Smolyakov, and M. Yagi, Phys. Plasmas **9**, 1659 (2002)
[4] Z. Gao, H. Sanuki, K. Itoh, and J.Q. Dong, Phys. Plasmas **10**, 2831 (2003)
[5] Z. Gao, H. Sanuki, K. Itoh, and J.Q. Dong, Phys. Plasmas **12**, 022502 (2005)
[6] J. Chowdhury, R. Ganesh, J. Vaclavik, S. Brunner, L. Villard, P. Angelino, Phys. Plasmas **16**, 082511 (2009)
[7] M. A. Beer, S. C. Cowley, and G. W. Hammett, Phys. Plasmas 2, 2687 (1995)
[8] J.W. Connor, R.J. Hastie, J.B. Taylor, Phys. Rev. Lett. **40**, 396 (1978)
[9] A.G. Peeters, Y. Camenen, F.J. Casson, W.A. Hornsby, A.P. Snodin, D. Strintzi and G. Szepesi, Comp. Phys. Comm., **180**, 2650 (2009)
[10] F.J. Casson, PhD thesis, University of Warwick (2011)
[11] R.E. Waltz, G.D. Kerbel, J. Milovich, Phys. Plasmas **1**, 2229 (1994)
[12] X. Lapillone, S. Brunner, T. Dannert, S. Jolliet and A. Marinoni et al., Physics of Plasmas, vol. **16**, num. 3, (2009)
[13] A.G. Peeters, D. Strintzi, Y. Camenen, C. Angioni, F.J. Casson, W.A. Hornsby, A.P. Snodin, Phys. Plasmas **16**, 042310 (2009)
[14] J. Chowdhury, S. Brunner, R. Ganesh, X. Lapillonne, L. Villard, and F. Jenko Phys. Plasmas 19, 102508 (2012)
[15] D. Told et al., Phys. Plasmas 15, 102306 (2008)
[16] A. Mishchenko, R. Hatzky and A. Koenies, Theory of Fusion Plasmas, Joint Varenna-Lausanne International Workshop, AIP Conference Proceedings vol. 871, page 395 (New York, 2006)